JOURNAL OF AIRCRAFT
Vol. 43, No. 2, March–April 2006

Coated Hot-Film Sensors for Transition Detection in Cruise Flight

Felix Hausmann* and Wolfgang Schröder†
RWTH Aachen University, 52062 Aachen, Germany

In this paper results of wind-tunnel experiments and flight tests that demonstrate the effectiveness of coated multisensor hot-film arrays using constant current anemometry to determine boundary-layer transition under cruise conditions are presented. The study focuses on the analysis of several coating procedures, materials, and coating thicknesses to improve mechanical durability and signal quality. After several numerical simulations and environmental resistance tests, for example, in climate chambers and low-speed flight experiments, wind-tunnel experiments and flight tests at transonic speeds are carried out. The numerous experimental and numerical investigations and flight tests in cooperation with the Deutsche Airbus GmbH on a Beluga airplane (300-600ST) show a 1-μm parylene layer covering the extremely sensitive hot-film sensors and conducting paths to be sufficiently robust to stand the environmental conditions in cruise flight for several months. Furthermore, flight tests at transonic speeds on the Mystere Falcon 20 E5 at an altitude up to 30,000 ft and Mach numbers up to 0.79 are conducted in a joint project with DLR Oberpfaffenhofen. Modified wing models are mounted under both wings of the Falcon. The surfaces are instrumented with coated hot-film arrays using 128 sensors. The tests on the Falcon prove parylene coated hot-film sensors to still possess the sensitivity to locate transition under real flight conditions.

Nomenclature

c	=	airfoil chord length, m
c_p	=	static-pressure coefficient
f	=	frequency, Hz
h	=	standard pressure altitude, ft
I	=	hot-film current, mA
Ma	=	Mach number
R	=	resistance, Ω
Re	=	Reynolds number based on airfoil chord
Re_γ	=	attachment-line momentum-thickness Reynolds number
r	=	nose radius of airfoil, m
u	=	freestream speed, m/s
α	=	angle of attack of airfoil, deg
α_F	=	angle of attack of Falcon aircraft, deg
β	=	angle of yaw of airfoil, deg
β_F	=	angle of yaw of Falcon aircraft, deg
γ	=	leading-edge sweep angle of airfoil, deg
ε	=	ellipticity of an equivalent ellipse
ν	=	kinematic viscosity, m^2/s

I. Introduction

THE interest in detecting boundary-layer transition is justified, among other applications, by the impact of the state of the flow on the performance of aircraft. To reduce the surface drag, the laminar-turbulent boundary-layer transition should occur as far downstream from the leading edge as possible. Analyses of the laminar flow concept predict fuel savings up to 20% (Ref. 1). Although transitional and turbulent boundary layers are tackled in numerous research studies, there is hardly any project that addresses the problem of predicting boundary-layer transition under free flight conditions.[2–5]

It is fair to say that the effects of freestream turbulence, noise, surface roughness, vibrations of the wing, etc. are not well enough understood to predict transition on wings in cruise flight neither numerically nor experimentally by wind-tunnel tests. Because of the strong influence of these phenomena on the transition process, an appropriately small, robust, nonintrusive measuring technique has to be developed such that data can be recorded and analyzed online at cruise flight conditions. Therefore, a resistant multisensor hot-film system is developed and tested first at wind-tunnel and then at free-flight conditions to determine online during cruise flight the location of transition and separation. This paper reports on a multisensor hot-film technique, which is resistant and yet sensitive enough to detect transition. The method can be part of a complete control system that could be used to optimize the shape of the wing during cruise flight.

The paper is organized as follows. First, numerous materials and coating procedures are analyzed, for example, by numerical simulations. Next, wind-tunnel tests are performed to investigate the dynamic response of coated hot-films and to detect transition under lab conditions. Finally, after having determined the most promising coating in long-term flight tests to check the mechanical stability, the new coated hot film will be used to determine transition under transonic flight conditions.

II. Coating Procedures and Materials for Multisensor Hot Films

To maintain a sufficient temporal resolution of the heated sensors and to simultaneously enhance the protective properties of the coating, numerous coating materials are scrutinized in terms of high mechanical loads, for example, resistance against impinging insects, ice crystals, etc., and material requirements, for example, water repellent, resistance against ultraviolet radiation, etc. Based on many years of experience in manufacturing multisensor hot-film foils, these new hot-film arrays are developed to withstand normal stresses as they occur under free-flight conditions.

First, the heat-transfer behavior and temporal resolution are numerically analyzed to limit the number of coating materials and to obtain more information on the material properties, layer thicknesses, and coating processes. Using a protective layer on the heated sensors, the heat emission and the temporal resolution are strongly reduced. However, the susceptibility of the sensors to these properties is necessary to record the intermittent measuring signals in the kilohertz range at transition. In the following, predictions are made for the steady and intermittent behavior of coated hot-film sensors with special attention on the impact of the material properties and thicknesses of the protective layers. For the three-layer

Presented as Paper 2004-1047 at the AIAA 44th Aerospace Sciences and Meeting and Exhibit, Reno, NV, 5–8 January 2004; received 28 February 2005; revision received 8 June 2005; accepted for publication 9 June 2005.

*Research Scientist, Institute of Aerodynamics, Wüllnerstr. zw. 5 u. 7; felix@aia.rwth-aachen.de.

†Professor, Department of Mechanical Engineering, Institute of Aerodynamics, Wüllnerstr. zw. 5 u. 7. Member AIAA.

hot film (protective layer hot-film foil substrate), a numerical procedure is developed, which iteratively solves the two-dimensional heat-conduction equation using finite differences. The heat transfer on the hot-film surface is defined by prescribing a heat-transfer coefficient. This leads to a very efficient software to analyze different coating materials. Using this method, fundamental findings regarding the signal detection sensitivity are obtained.

Assuming steady boundary conditions, the temperature distributions within the hot film are determined for different parameters. Using materials such as polyimid and large layer thicknesses, for example, 12 μm, only a small increase in the temperature difference between the surface of the hot film and the airflow, located at $y = 0$, occurs, yielding an almost negligible heat transfer and very poor temporal resolution of the hot-film sensor (Fig. 1). However, when the hot film is covered by a high thermal conductive coating (SiO_x), a temperature distribution similar to that of an unprotected hot film is achieved (Fig. 2), that is, a strong temperature gradient is determined at $y = 0$.

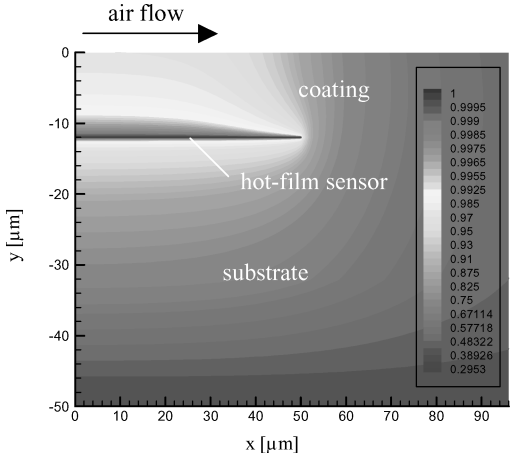

Fig. 1 Temperature distribution for the hot film covered with a polyimid protective layer (12 μm).

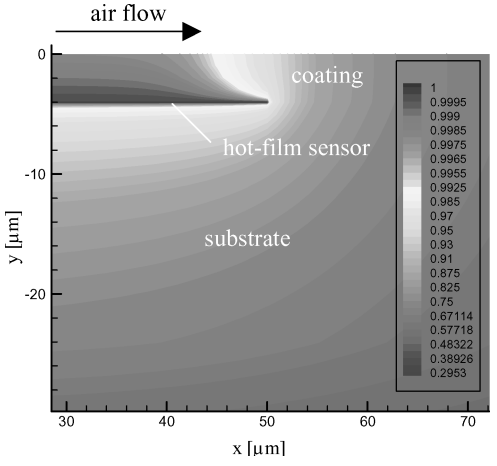

Fig. 2 Temperature distribution for the hot film covered with a SiO_x layer (4 μm).

Subsequently, the temporal behavior of various hot films is investigated by prescribing a heat-transfer coefficient that sinusoidally depends on time. The frequency response is represented in a Bode diagram that contains the power spectral density function as a function of frequency. The sensitivity of the hot-film probe depends on the material, the thickness of the protective layer, and that of the substrate. Figure 3 shows the SiO_x-covered hot film to have a frequency response almost identical to that of the unprotected sensors.

Based on those findings of numerous numerical analyses,[6] the materials SiO_x, parylene, and polyimid in conjunction with protective layer thicknesses, which satisfy the requirements of good heat conductivity and temporal resolution, are selected for further investigations. Moreover, different thin-layer application procedures [physical vapor deposition, chemical vapor deposition (CVD), chemical vapor varnishing (CVV), low-temperature vacuum coatings, compressed air spraying procedure, etc.], materials (ceramics, diamond-similar carbon layers, metals, lacquers, epoxy resins, polymers, foils, etc.), layer thicknesses (100 nm to 19 μm), pretreatments (low-pressure plasma and alkaline degreasing procedures), and compound systems are examined. Because the hot-film arrays can cover an area of up to 1.25×0.38 m, the coated physical structures must be allowed to be evenly and pin free applied on a large surface to ensure an identical temporal resolution with different sensors and to prevent damage to the sensors caused by short circuits and/or oxidization by penetrating humidity.

Because of the sensitivity of the extremely thin nickel sensors and the small temperature resistance of the transparent material (polyimid), a number of coating processes, such as CVD, CVV, and some compressed air spraying procedures, cannot be applied because those methods damage or destroy the transparent material and/or the sensors during the pretreatment phase (Fig. 4).

Because the multisensor hot-film arrays are applied to curved surfaces, say, wings, pylons, etc., they have to be very flexible.

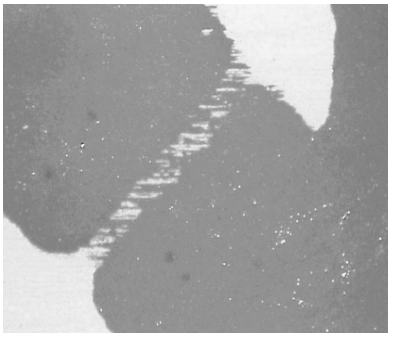

Fig. 4 Microscopic picture of a damaged hot film.

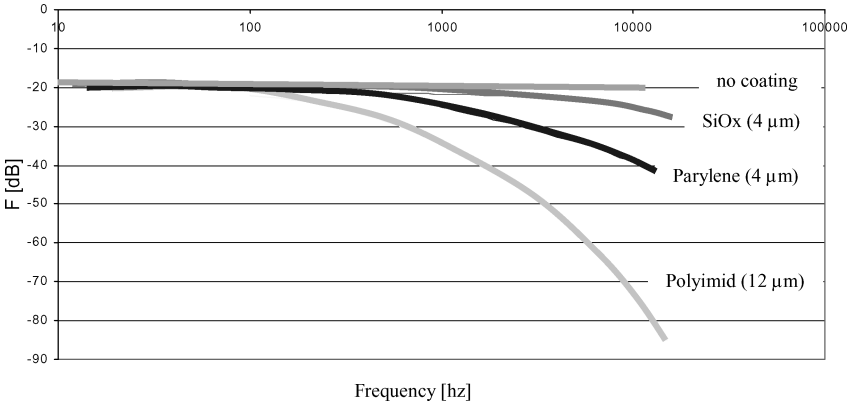

Fig. 3 Bode diagram of the frequency response of differently coated hot films.

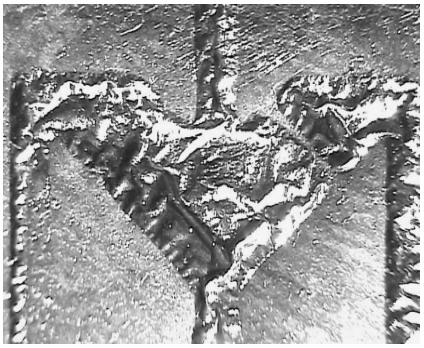

Fig. 5 Microscopic picture shows the insufficient adhesion of parylene and zircon nitride layers on copper conductive strips, a nickel sensor, and a polyimid foil.

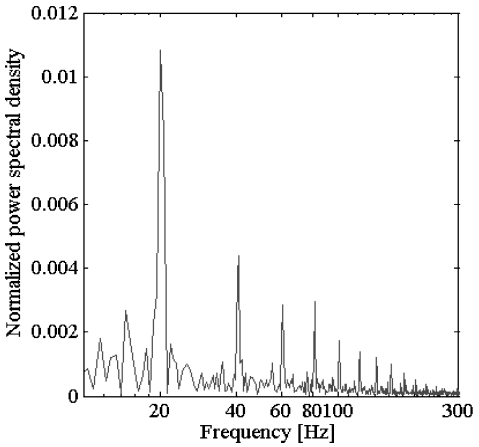

Fig. 6 Power spectra of a 2-μm parylene-coated hot-film signal at sine-wave excitation of $f = 20$ Hz.

Therefore, coatings like lacquers, metals, and epoxy resins can no longer be used. Furthermore, materials like ceramics, diamond-similar carbon layers, and polymers are of no use because some of the hot-film layers do not stick together and come off (Fig. 5).

Simultaneously to the laboratory tests just discussed, initial environmental resistance tests with the coated multisensor hot-films are performed. To simulate certain cruise-flight conditions, the films are exposed to temperatures ranging from -50 to $+90^{\circ}$C and ultraviolet radiation for several weeks in climatic chambers.

The overall analysis of the results of the aforementioned test series shows the coatings parylene and SiO_x to meet at best the requirements of sensitivity, robustness, flexibility, and resistance. For this reason, these materials are primarily used in further wind-tunnel and flight tests.

III. Dynamic Response

Next, wind-tunnel tests are performed to investigate the frequency response of coated hot-film sensors. A local perturbation was introduced in the surface of a flat plate by a harmonic point source. The leading edge possessed an elliptical shape to avoid separation. The flow is excited by single-frequency sine waves through a disturbance generator. The sensitivity of coated hot-film sensors flush mounted in the flat plate to minimize sensor-induced disturbances and placed 22 mm downstream from the harmonic point source is investigated by analyzing time traces and power spectral density distributions (Fig. 6). The sine-wave excitation of 20 Hz is clearly detected by the parylene-coated hot-film sensor.

The results are compared with pure hot-film and hot-wire measurements. A general frequency response of different measuring devices is presented in Fig. 7. The frequency responses of coated and pure hot-film sensors as well as of a hot wire normalized by the amplitude of the 20-Hz excitation are compared for several single-frequency sine waves (100–600 Hz). These results show parylene-coated hot-film sensors to be the best solution as far as sensitivity is concerned because the parylene-coated sensor possesses at frequencies less than 200 Hz a similar frequency resolution as the uncoated hot film. The following experiments for transition detection will show whether or not the protected hot films have the sensitivity to detect transition.

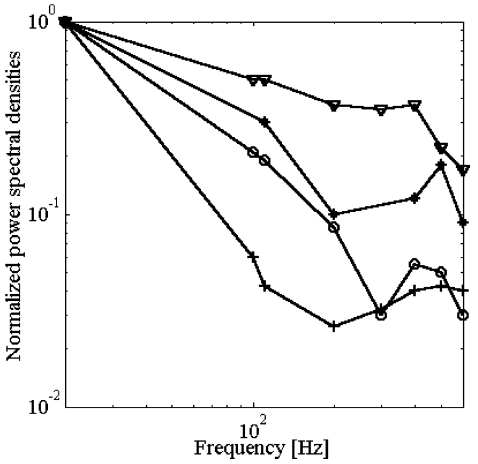

Fig. 7 Normalized frequency responses for several single frequency sine-wave excitations and various measurement techniques ($\triangledown$, hot-wire; $*$, pure hot-film; $\bigcirc$, 2-μm parylene-coated hot-film; and +, 12-μm polyimid-coated hot film).

IV. Wind-Tunnel Experiments for Transition Detection

In the trisonic wind tunnel the flow over the LVA - 1a airfoil is used as a test problem to detect transition with coated multisensor hot-film arrays.

The wind tunnel possesses a measurement cross section of 40×40 cm^2 and is equipped with adaptive upper and lower walls to reduce the interference between the airfoil and the measuring chamber walls. The experiments are performed at Mach numbers ranging from 0.5 to 0.76 in 0.05 increments up to Mach 0.7 and then in 0.02 increments. Because at higher Mach numbers the transition is influenced by shock-induced separation, the investigation of the transition process is essentially limited by a maximum freestream Mach number of 0.72. Constant-current anemometry (CCA) and constant-temperature anemometry (CTA) multisensor hot films with 20 single sensors are applied to the airfoil. The sensors are transversely oriented to the main flow direction and diagonally arranged with a spacing of 3 mm (1.5% chord). The dimensions of the sensors are $0.09 \times 4 \times 0.0025$ mm^3.

We now turn to the discussion of the transition results with and without coating. The transition locations detected by the hot-film technology are verified by shear-stress sensitive paint distributions.[7] The investigation of the liquid crystal pictures shows at Mach numbers ranging from 0.65 to 0.72 and an angle-of-attack of 1 deg a transition area without any separation.[8,9]

For the hot-film technique the timescale, the standard deviation, and the skewness of the voltage fluctuations of the measuring signals are used to determine the transition position (Fig. 8). Because the transitional boundary layer is characterized by a strong intermittency, fluctuations of large amplitude occur that cause a significant rise of the standard deviation, which vanishes in the fully turbulent state. The skewness distribution shows a maximum, followed by a sign change, that is, an x intercept, and a minimum at the end of the transition area.[10,11] These criteria, that is, the increased standard deviation and the x intercept of the skewness, are clearly visible in the CTA measurements for the uncoated hot film in Fig. 8. At an angle of attack $\alpha = 1$ deg and a Mach number $Ma = 0.70$, the transition sets in at approximately 53% and ends at approximately 68% chord length. The CCA measurements yield a similar result for the transition area. Figure 9 shows that at $Ma = 0.70$ and $\alpha = 1$ deg the transition area can be definitely detected between 53 and 68% chord.

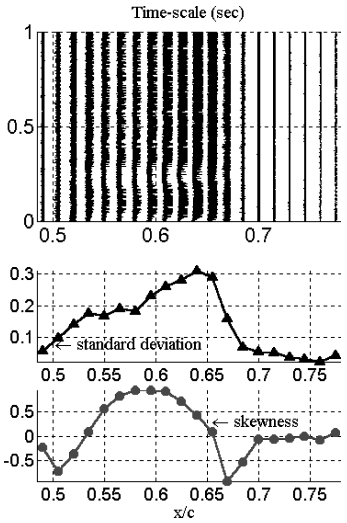

Fig. 8 CTA measurement: transition detection using a multisensor hot-film array without coating for $Ma = 0.7$, $\alpha = 1$ deg. Timescale and statistical analysis are presented as a function of chord.

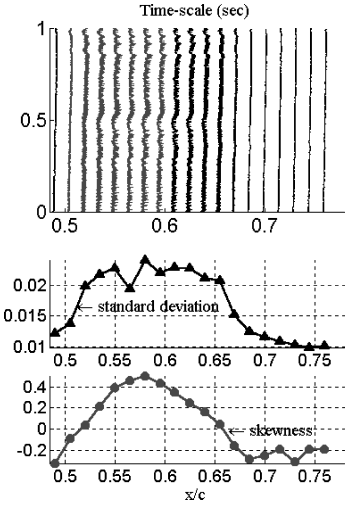

Fig. 9 CCA measurement: transition detection using a multisensor hot-film array without coating for $Ma = 0.7$, $\alpha = 1$ deg. Timescale and statistical analysis are presented as a function of chord.

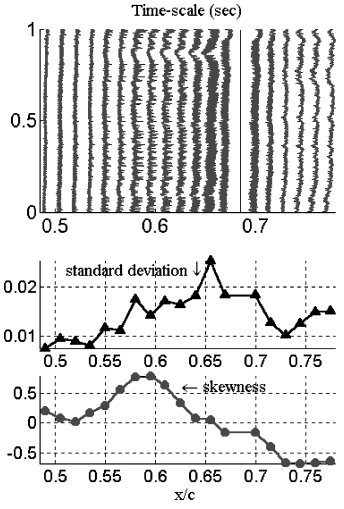

Fig. 10 CCA measurement: transition detection using a multisensor hot-film array with 4-μm SiO_x coating for $Ma = 0.7$, $\alpha = 1$ deg. Timescale and statistical analysis are presented as a function of chord. Sensor 14 is defective.

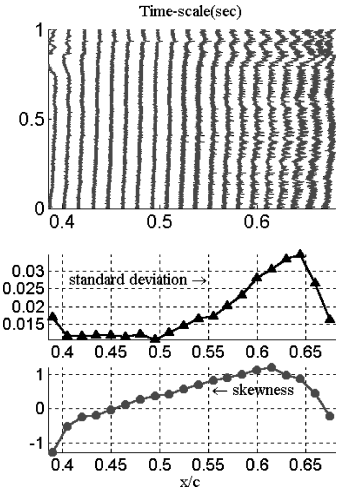

Fig. 11 CCA measurement: transition detection using a multisensor hot-film array with SiO_x coating and 0.4-mm-wide sensors for $Ma = 0.7$, $\alpha = 1$ deg. Timescale and statistical analysis are presented as a function of chord. The hot film is shifted upstream by 10% chord.

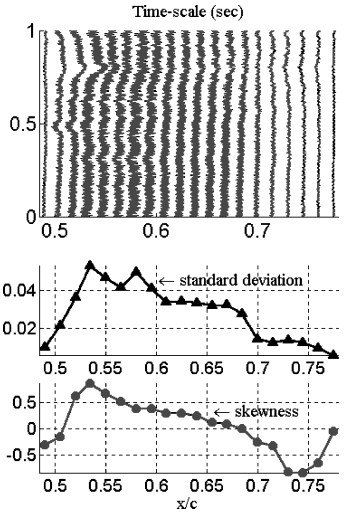

Fig. 12 CCA measurement: transition detection using a multisensor hot-film array with parylene coating for $Ma = 0.7$, $\alpha = 1$ deg. Timescale and statistical analysis are presented as a function of chord.

The following results refer to CCA measurements for coated multisensor hot-film arrays. The findings of the CTA investigations are not shown here because the distributions are more or less alike. We start by discussing the results of the 4-μm SiO_x coating. The distributions of the standard deviation and the skewness evidence the transition area to be between 53 and 69% chord (Fig. 10). To further enhance the robustness of the hot-film sensors, the width of each sensor is increased from 0.09 to 0.40 mm. Although this modification causes a slight reduction in the sensor sensitivity, the skewness distribution indicates the end of the transition regime at 68% chord because the zero-line intersection occurs somewhat upstream at 0.66 (Fig. 11). Because the resistances of wider sensors (approximately 12 Ω each) can be manufactured more accurately, the increase of the skewness and the standard deviation is smoother in Fig. 11 compared to other findings.

Figure 12 gives evidence that the hot-film sensors protected by a 4-μm parylene coating yield a transition area of almost the same size and location compared with the SiO_x data. The skewness distribution defines the onset of a fully turbulent boundary layer at approximately 70% chord.

Unlike the SiO_x and the parylene coating, the polyimid coating prevents the hot-film sensors to detect the transition location.[6] This is because of the unsatisfactory sensitivity of the system evidenced by the power spectral densities (Figs. 3 and 7).

V. Flight Experiments at Low Speeds

Besides climatic chamber and wind-tunnel experiments, the hot films have to undergo low-speed flight tests. Figure 13 shows various hot films applied to the leading edge of a Piper 28 airplane. Based on an eight-month test, that is, the sensors remain on the wing for 35 weeks and have to stand a flight time of more than 400 h at an altitude of up to 3000 m, an average airspeed of 100 kn, and an air temperature of -10°C, the following findings are obtained. The hot-film sensors protected by a parylene or polyimid layer are okay, that is, absolutely no damage can be detected (Fig. 14), whereas the uncoated sensors suffer extremely from the environmental conditions such that they can no longer be used to measure transition or separation (Fig. 15).

Fig. 13 Multisensor hot-film arrays on a Piper 28 airplane (altitude, 3000 ms; airspeed, 130 kn; air temperature, −10°C). From top to bottom: ZnO-coated hot film, polyimid-coated hot film, parylene-coated hot film, SiO_x-coated hot film, and two pure hot films.

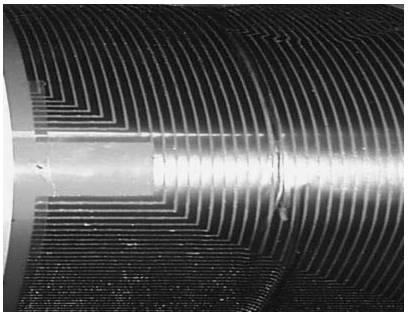

Fig. 14 Parylene-coated hot film looks perfect after a 20-week flight test.

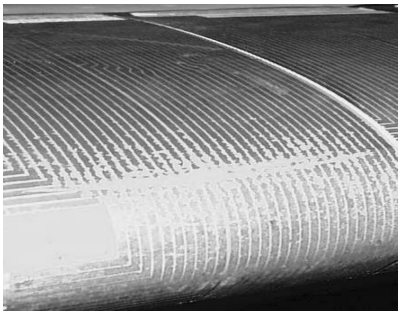

Fig. 15 Pure hot film damaged after a 20-week flight test.

VI. Resistance Experiments at Transonic Flight

In the first phase of the flight experiments at transonic speeds, additional investigations at altitudes up to 33,000 ft are performed on an Airbus Beluga (300-600ST). They focus on the development and tests of robust multisensor hot-film arrays for long time use under cruise flight conditions. A thin metal plate is covered with several coated hot-film arrays and mounted above the cockpit of the airplane, where the environmental impact is extremely high (Fig. 16). The investigations show a 1-μm parylene layer covering the extremely sensitive hot-film sensors and conducting paths to be sufficiently robust to stand the environmental conditions in cruise flight for several months (Fig. 17). The uncoated hot film and other hot films protected by different materials are damaged such that they can no longer be used for transition detection (Figs. 18 and 19). Thus, parylene-coated hot films are used for the final cruise flight experiments. Furthermore, the following flight experiments will be performed with protective layer thicknesses of 1 μm, instead of thicknesses of 2 and 4 μm tested in the wind tunnel (see Secs. III and IV) because the smaller the thickness the higher the sensitivity to detect transition.

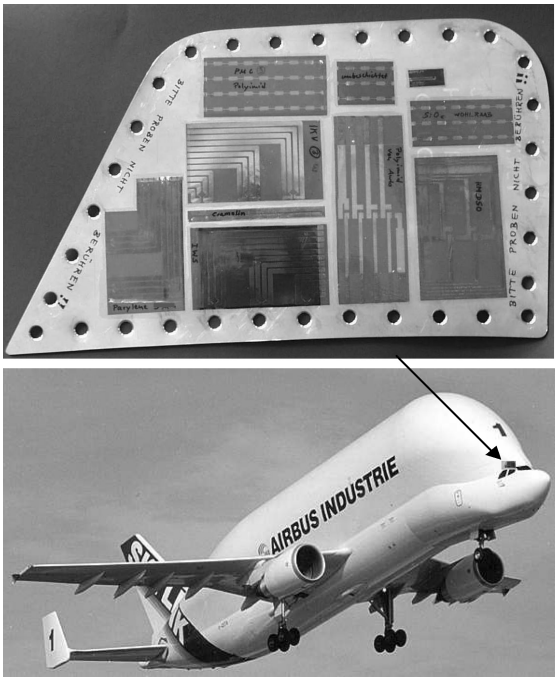

Fig. 16 Several hot films mounted on an Airbus Beluga airplane. From top to bottom and left to right in the upper figure: parylene-coated hot film (1 μm), polyimid-coated hot film (12 μm), SiO_x-coated hot film (300 nm), hot film with lacquer layer (5 μm), hot film with diamond-like carbon layer (DLC, 100 nm), pure hot film, polyimid-coated hot film (12 μm), pure hot-film sensor from TaoSystems (Senflex), SiO_x-coated hot film (200 nm), hot film with SiO_x layer (100 nm).

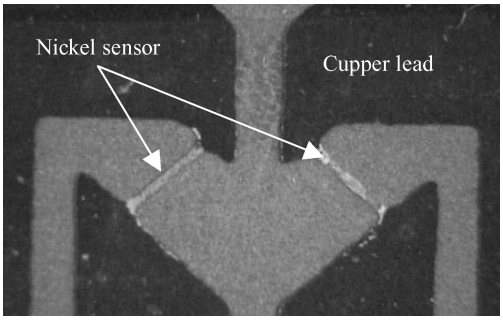

Fig. 17 Microscopic picture: parylene (1-μm)-coated hot-film sensors are in perfect condition after a two-month flight test.

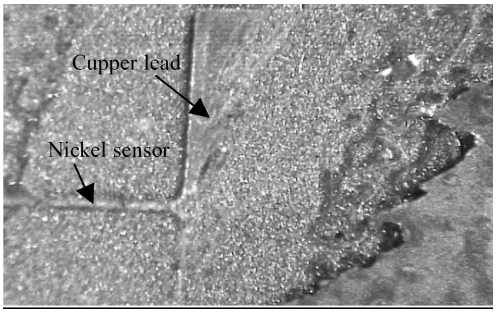

Fig. 18 Microscopic picture: SiO_x (100-nm)-coated hot film severely damaged after a two-month flight test.

VII. Transition Detection at Transonic Flight

Finally, flight tests at transonic speeds are conducted in collaboration with the DLR Flight Facility Oberpfaffenhofen flying the Mystere Falcon 20 E5 at an altitude of up to 30,000 ft and a maximum Mach number of $Ma = 0.79$. Modified wing models are mounted under both wings of the Falcon (Fig. 20). The surfaces of the airfoils were instrumented with parylene-coated hot-film arrays using 128 sensors to record data during flight.

A. Aircraft and Hardware Description

The Mystere Falcon 20 E5 D-CMET is a twin jet aircraft with a pressurized cabin and several modifications for atmospheric research. The standard data-acquisition frequency for the complete data set (temperature ϑ, pressure, humidity, etc.) and all flight parameters (velocity u, height h, angle of attack α_F, angle of yaw β_F, etc.) is 10 Hz. A new leading-edge model, based on an NLF(1)-0416 profile and a natural laminar flow glove used on a transport aircraft,[12] is specially designed to fly on the Falcon 20 E5 and to ensure boundary-layer transition at transonic flight conditions. Two wing models of sweep angle $\gamma = 20$ deg covering the front part of already existing pylons are mounted 10% chord downstream of the leading edge of both Falcon wings. The overall chord length of the airfoil mounted underneath the Falcon wing was 0.960 m, its thickness at the base was 0.104 m, and its height was 0.428 m.

The transition on swept wings is induced either by the Tollmien–Schlichting instability, crossflow instability, which is caused by strong spanwise pressure gradients, or an attachment-line contamination. To avoid attachment-line transition, it is necessary to keep the Reynolds number Re_γ based on the attachment-line momentum thickness in the range below 100 (Ref. 13). Following Pfenningers experimental results,[14,15] an approximate relationship for Re_γ is given by

$$Re_\gamma = 0.404 \cdot \sqrt{\frac{u \cdot r \cdot \sin^2 \gamma}{(1+\varepsilon) \cdot \nu \cdot \cos \gamma}}$$

For the flight tests the maximum Reynolds number Re_γ is 24, resulting in a laminar and stable attachment-line boundary layer.

Wind-tunnel measurements on a scaled model (1:5.65, Fig. 21) at transonic airspeeds are used to predict the pressure distribution and transition location because of the Tollmien–Schlichting instabilities and, thus, to appropriately position the hot-film sensors for the free-flight experiments. Besides, the hot-film arrays on the wind-tunnel model are used to test and optimize the CCA right before the flight tests.

Depending on the freestream velocity and the angle of attack, the minimum pressure point on the surface is located at about $x/c = 0.15$ (Fig. 22). That is, the Tollmien–Schlichting instabilitiy is subcritical up to approximately $x/c = 0.15$. Another extremum at $x/c \approx 0.45$ is caused by the interaction of the flow over the wing and the mounted wing models.

Crossflow instabilities arise from a dynamic instability of the spanwise pressure profile generated by the three-dimensional character of the mean flowfield. Although the sweep angle of the airfoil $\gamma = 20$ deg is rather low, there is still a chance that at certain yaw angles β_F and angles of attack α_F crossflow vortices appear upstream of the minimum pressure location. Moreover, an interaction between the Tollmien–Schlichting waves and crossflow vortices generated in the pressure recovery region is likely to occur.[16] For this reason, sensors are positioned between the leading edge and 50% chord to ensure that the transition region is covered.

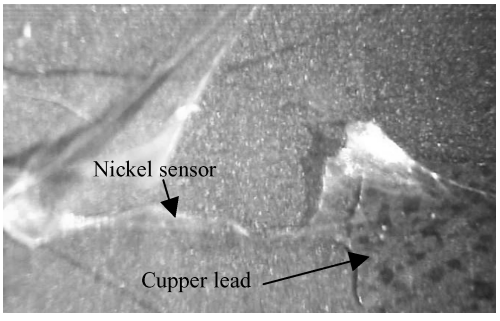

Fig. 19 Microscopic picture: polyimid coating (12 μm) peeled off from the hot film after a two-month flight test.

B. Instrumentation

The starboard and port model contours are identical and constructed from a 2-mm glass-fiber laminate sandwich covered with

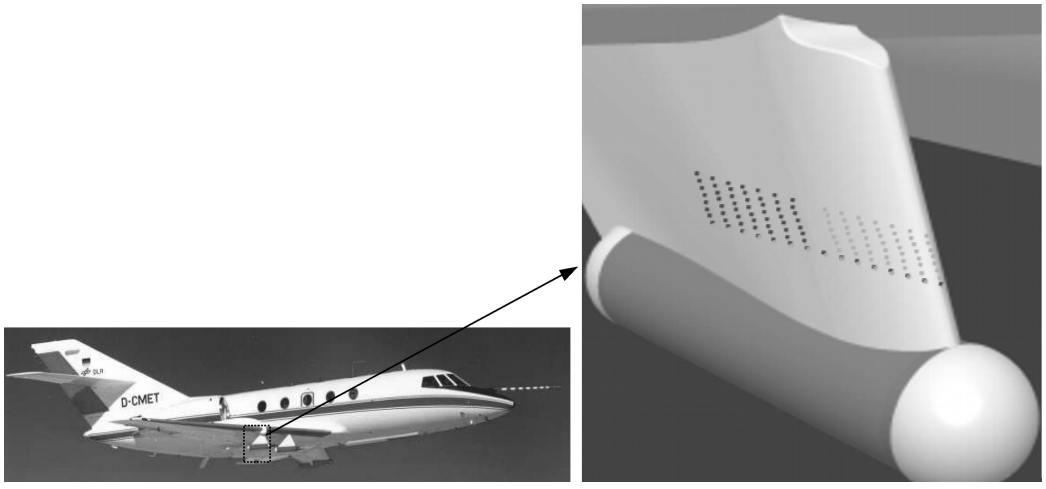

Fig. 20 Geometry and sensor arrangement of the wing model mounted underneath the main wing.

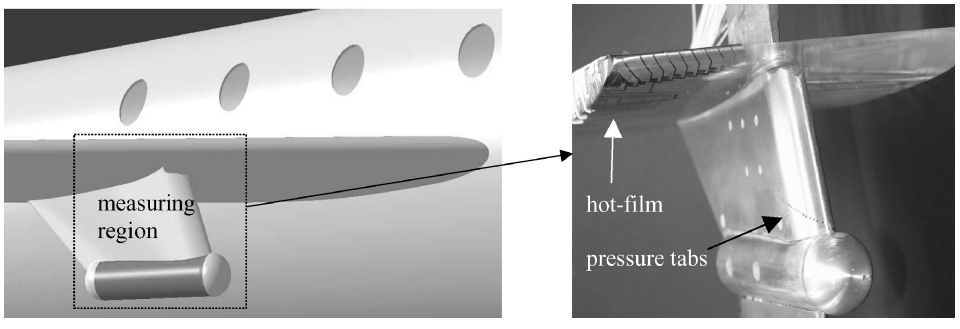

Fig. 21 Wind-tunnel model with pressure taps and hot-film arrays.

a high-quality surface finish. The sensor foils are centrally placed covering the leading edge completely. Both multi-element hot-film sensor sheets used in these tests consist of two arrays of 64 parylene-coated hot-film sensors, which are 4 mm long, 0.1 mm wide, and 0.25 μm thick, each of which is on a polyimid substrate. The sensors are transversely oriented to the main flow direction, and eight sensors are arranged in a diagonal pattern with a spacing of 34 mm to minimize the thermal influence of the upstream sensors. Starboard and port sensor arrangements are slightly different to cover a larger measuring zone. The unheated resistance of the sensor elements possess a nominal value $R = 18\,\Omega\,(\pm 15\%)$ on the ground and drop to approximately $R = 12\,\Omega$ at $h = 30{,}000$ ft, where the static air temperature is 226 K.

In the experimental setup the sensor leads are soldered onto connector plug wires, which are routed through narrow slots on the surface far away from the measuring zone into the wing model such that a completely smooth measuring zone is achieved. Because only a limited number of cable connections is available, a switching relay is used to record all of the 128 sensors, 64 sensors of which are simultaneously recorded. Cable connections, switching relays, and the connector plugs to the cables are installed in the interior of the wing model. Coaxial cables running through both wings connect the wires to the measuring system. The hot-film data are recorded onboard using a CCA. Especially under cruise flight conditions the CCA has the strong advantage of less instrumental effort to operate 128 sensors because several sensors can be heated by only one common constant-current source. Eight sensors are connected in series with one out of 16 individual current sources to reduce the number of conducting paths. Depending on the variable airflow conditions, the heating current is adapted in the range of $I = 35$–90 mA.

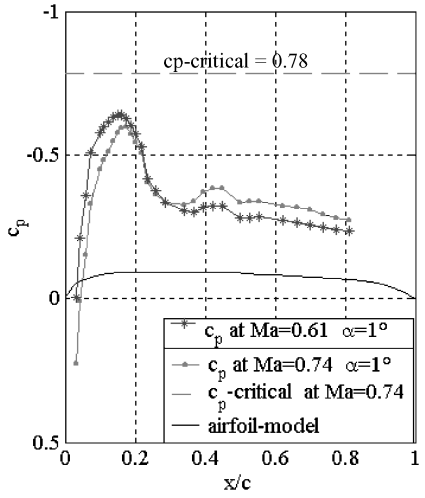

Fig. 22 Pressure distributions for $Ma = 0.69$ and 0.74 at $\alpha = 1$ deg; the cross section is defined by the pressure holes in Fig. 21.

For each new airflow condition an offset voltage is subtracted, and the fluctuating remaining voltage is amplified. Thus, the probe sensitivity is guaranteed by offset-compensated differential inverting amplifiers. Each sensor voltage is filtered by a 5-kHz low-pass filter, recorded by a transient recorder, and the voltage fluctuations can be viewed online on the laptop via an Ethernet interface. The CCA system, transient recorder, laptop, and voltage supply for the switching relays are integrated into a 19-in.-rack, whose structure is stress analyzed and electrical interference resistance is optimized for cruise flight conditions. The CCA system is completely computer controlled by an implemented RS 232 interface using an in-house-developed Labview program. The memory enables measurement times of up to several hours with a sample rate of 10 kHz and a resolution of 16 bit. The overall measuring accuracy during the flight tests is 0.5% of the input voltage, which is automatically adjusted to ± 5 V for the offset-compensation and to ± 1.25 V for the measurements. Frequencies up to 5 kHz can be resolved, which is reasonable for this application. All research and air data parameters are digitally encoded and simultaneously recorded onboard.

C. Results and Discussion

Flight data are obtained at altitudes up to 30,000 ft during stabilized flight. To properly design the system, the reset, current setting, and autozeroing of the hot-film sensors are done after each individual

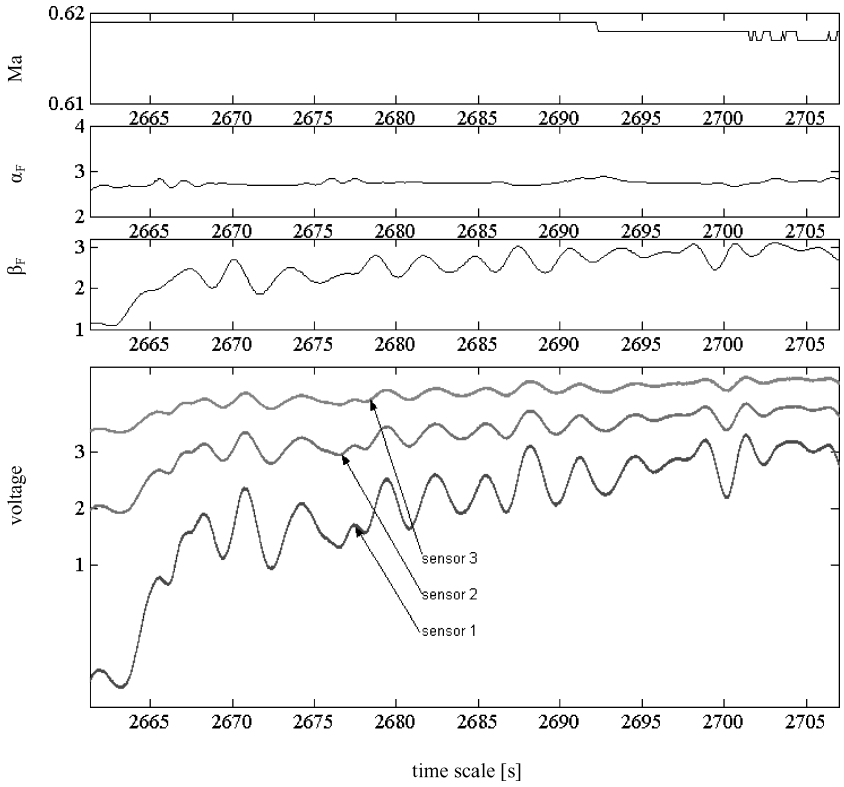

Fig. 23 Mach number Ma, angle of attack α_F, angle of yaw β_F, and time histories of 1-μm parylene-coated hot-film sensors in stabilized flight as a function of time; the voltage distributions of the first three sensors of the starboard hot-film array are shown.

Fig. 24 Starboard airfoil with parylene-coated multisensor hot-film array in flight.

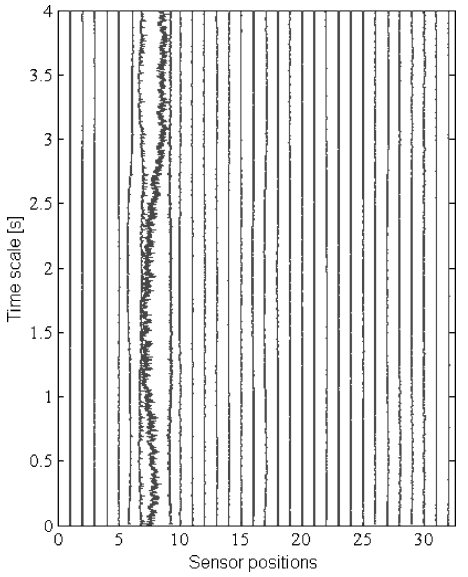

Fig. 25 Parylene-coated hot-film time histories in cruise flight at $Ma = 0.27$ and $\alpha = 1.9$ deg on the port-mounted airfoil ($\beta = 5$ deg, $h = 12{,}500$ ft, $\vartheta = -6°$C). Sensor 4 is defective.

flight maneuver. The Reynolds number based on the wing chord at the center section varies between $Re = 3.9 \times 10^6$ and 6.1×10^6.

In the following, we discuss the flight data that are obtained in the subsonic and transonic flow regime, that is, at $0.27 \leq Ma \leq 0.79$. Moreover, the angle of yaw and angle of attack are varied in the range of approximately ± 2 deg to test and demonstrate the quality of the hot-film sensors to detect transition under real flight conditions. A typical time history for the coated hot-film sensors in flight is shown in Fig. 23. When the angle of yaw β_F of the Falcon aircraft is increased, the angle of attack α of the starboard-mounted wing section also grows. This causes a growth of the measurement signals of the starboard hot-film sensors, indicating an increased airspeed at the leading edge of the wing section (Fig. 24). Furthermore, the hot-film signals follow a roll-yaw oscillation for a time period of about 40 s. Different amplitudes occur because of slightly differing sensor resistances ($R_1 = 20{,}1\ \Omega$; $R_2 = 18{,}1\ \Omega$; $R_3 = 17{,}6\ \Omega$) and larger $\Delta u/\Delta\alpha$ values at the leading edge than further downstream.

By analyzing the high-frequency signals of the hot-film sensors, the state of the boundary layer is determined. The timescale, the standard deviation, and the skewness of the voltage fluctuations of the measuring signals are used to determine the transition position. Independent of the transition mechanism, the transitional boundary layer is characterized by a strong intermittency. Fluctuations of large amplitude occur, which are illustrated in the hot-film time histories in Fig. 25 and in the enlargement for a flight Mach number of $Ma = 0.27$ in Fig. 26.

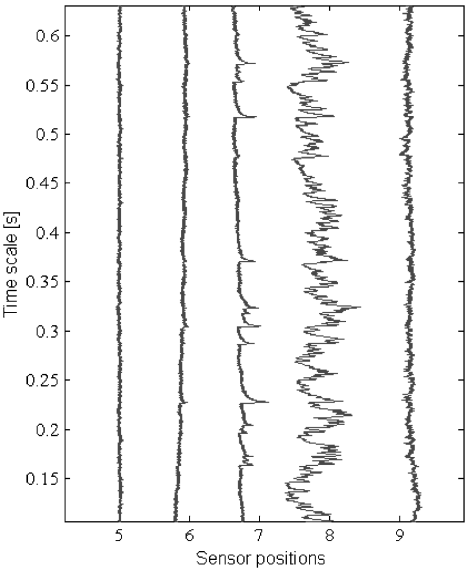

Fig. 26 Enlargement of the transition regime shown in Fig. 25.

Standard deviation and skewness distributions allow a comparison with the Gaussian distribution and are used to detect transition. Figure 27 shows the measurements on the port-mounted airfoil of the first 32 hot-film sensors of the parylene coated hot film at $Ma = 0.27$. In the transitional state, the intermittent boundary layer alternates between laminar and turbulent state with equal probability, which leads to bimodal probability distribution of the velocity close to the wall and a zero crossing of its skewness between sensor 8 ($x/c = 0.241$) and sensor 9 ($x/c = 0.277$). This case indicates the center of the transition region. If the onset of transition is defined as the first occurrence of turbulent spikes, the skewness gives suitable information through a local maximum caused by a strongly deformed probability distribution. Hence, at $Ma = 0.27$ and $\alpha = 1.9$ deg the onset of transition is located at $x/c = 0.205$ (sensor 7). The end of the transition region is indicated by a local minimum of the skewness distribution at $x/c = 0.277$ (sensor 9), caused by negative peaks in the sensor signal. Thus, the transition region extends over at least 7% chord.

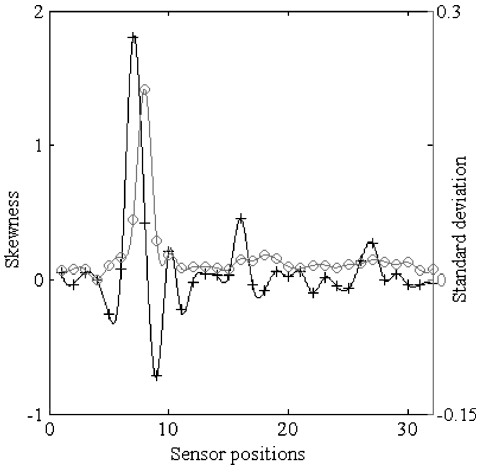

Fig. 27 Parylene-coated hot film on the port-mounted airfoil; standard deviation (○) and skewness distribution (+) in cruise flight at $Ma = 0.27$ and $\alpha = 1.9$ deg. Sensor 4 is defective.

Figure 28 shows time histories for the first 32 sensors of the port-side applied hot-film array at $Ma = 0.52$ and $\alpha = 1.6$ deg. It

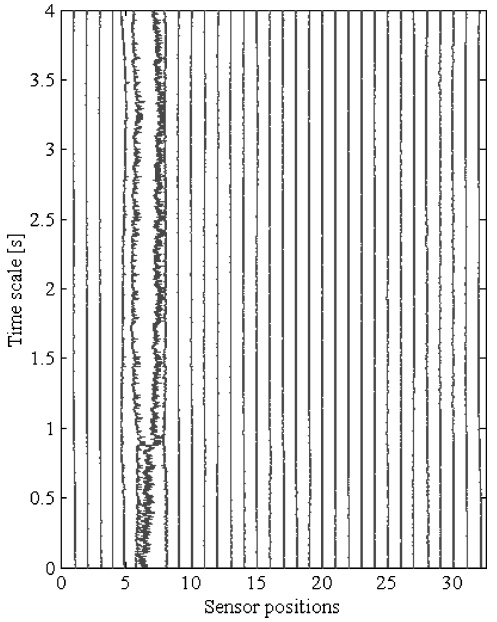

Fig. 28 Parylene-coated hot-film time histories in cruise flight at $Ma = 0.52$ and $\alpha = 1.6$ deg of the port-mounted wing model ($\beta = 4$ deg; $h = 16{,}700$ ft; $\vartheta = -18°$C). Sensor 4 is defective.

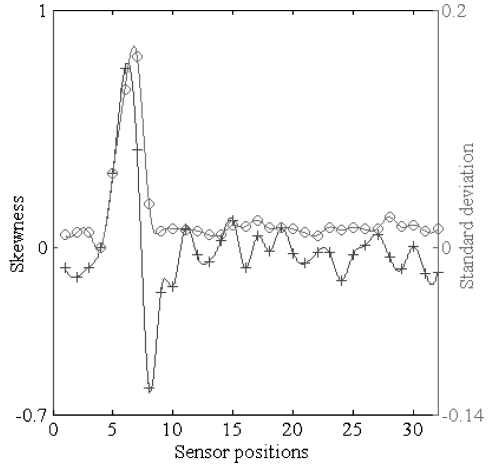

Fig. 29 Parylene-coated hot film on the port-mounted airfoil; standard deviation (○) and skewness distribution (+) in cruise flight at $Ma = 0.52$ and $\alpha = 1.6$ deg. Sensor 4 is defective.

illustrates the extent of turbulent flows from single turbulent spots at sensors 5 ($x/c = 0.134$) and 6 ($x/c = 0.169$) to a rather turbulent flow at sensor 7 ($x/c = 0.205$). Finally, negative spots occur indicating the end of the transition at sensor 8 ($x/c = 0.241$). From the analysis of the skewness distribution, it can be concluded that the transition sets in at $x/c = 0.169$ and ends at $x/c = 0.241$ (Fig. 29). High-amplitude fluctuations between sensors 5 and 9 increase the standard deviation significantly. The point of 50% intermittency, that is, the x intercept of the skewness distribution, is located at about 1% chord downstream of sensor 7, that is, at $x/c = 0.215$, and correlates with the maximum of the standard deviation.

For higher Mach numbers at similar angles of attack α, the transition area moves further upstream thereby increasing the fully turbulent flow region. Figure 30 illustrates the higher voltage fluctuations at a Mach number of $Ma = 0.79$ and $\alpha = 1.6$ deg at sensor 5 ($x/c = 0.134$) and sensor 6 ($x/c = 0.169$). The transition is evidenced by the distributions of the standard deviation and the skewness for the coated hot film in Fig. 31. Because the transition regime becomes smaller and sensor 4 is defective because of the manufacturing process, the beginning of transition cannot be identified as clearly as at lower Mach numbers. Nevertheless, the maximum value of the standard deviation and the zero-line interception of the

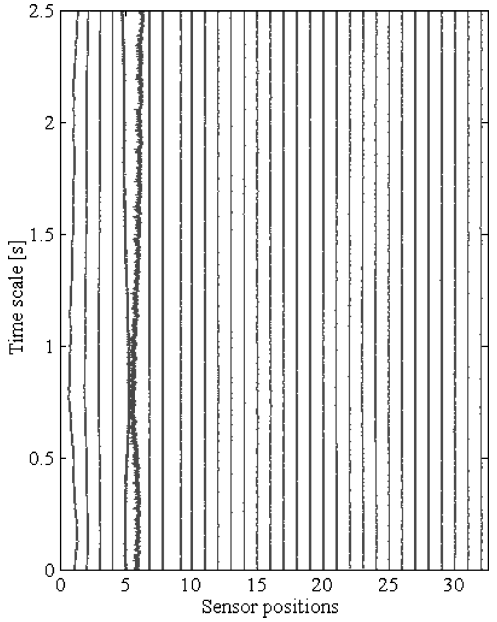

Fig. 30 Parylene-coated hot-film time histories in cruise flight at $Ma = 0.79$ and $\alpha = 1.6$ deg of the port-mounted wing model ($\beta = 2$ deg; $h = 30{,}500$ ft; $\vartheta = -49°$C). Sensor 4 is defective.

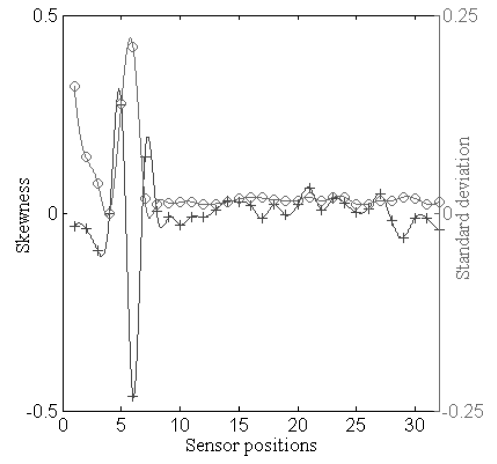

Fig. 31 Parylene-coated hot film on the port-mounted wing model; standard deviation (○) and skewness distribution (+) in cruise flight at $Ma = 0.79$ and $\alpha = 1.6$ deg. Sensor 4 is defective.

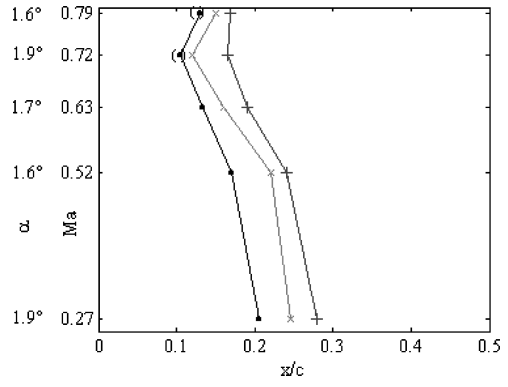

Fig. 32 Location and extent of the transition region as a function of Mach number and angle of attack: ●, begin of transition; ×, center of transition; +, end of transition; (○), extrapolation caused by defective sensor 4.

skewness distribution evidences the center of the transitional regime, where the intermittency factor is 0.5, to be located at approximately 2% chord upstream of sensor 6, that is, at $x/c = 0.149$.

The transition region for different Mach numbers at angles of attack of the wing models in the range of 1.6 deg $\leq \alpha \leq$ 1.9 deg are shown in Fig. 32. The influence of the Mach number on the transition position and its extent is quite evident. At a Mach number of $Ma = 0.79$, the skewness distribution yields an upstream shift of the transition onset of about 10% compared to that at $Ma = 0.27$ and a reduction of the streamwise extension from 8 to 4% chord. At $Ma = 0.79$ the transition sets in further downstream than at $Ma = 0.72$ because the smaller angle of attack leads to a less pronounced negative pressure gradient and a more downstream located suction peak. Hence, the instabilities start to grow further downstream from the leading edge of the wing model.

VIII. Conclusions

Numerical investigations, environmental resistance tests, wind-tunnel experiments, numerous flight experiments on a Piper PA 28 airplane, an Airbus Beluga, and subsequent frequency analyses have shown 1-μm parylene-coated hot films to yield the best results as far as robustness and sensitivity are concerned. Hot films without any coating cannot be used for measurements in long-term flight tests. The robust multisensor parylene-coated hot-film arrays and a newly developed automated constant-current-anemometer measuring system have been used to determine transition in cruise flight at Mach numbers up to $Ma = 0.79$ and altitudes up to 30,000 ft on a Mystere Falcon 20 E5. These flight tests have evidenced the coated hot-film arrays to be able to reliably detect transition under real cruise flight conditions.

Acknowledgments

The authors like to thank the German Research Association DFG and the German Aerospace Center DLR for making this study possible. The cooperation with several companies and research institutes as to flight tests and manufacturing of hot-film coatings is also gratefully acknowledged.

References

[1]Dallmann, U. Ch., "Identification and Modelling of Transition Scenarios in Boundary-Layer Flows—Recent Results Obtained at DLR Göttingen," *Fourth ECCOMAS Computational Fluid Dynamics Conference*, edited by K. D. Papailious, D. Tsahalis, J. Periaux, C. Hirsch, and M. Pandolfi, Vol. 2, Wiley, New York, 1998, pp. 118–125.

[2]Bake, S., Meyer, D. G. W., and Rist, U., "Turbulence Mechanism in Klebanoff-Transition. A Quantitative Comparison of Experiment and Direct Numerical Simulation," *Journal of Fluid Mechanics*, Vol. 459, 2002, pp. 217–243.

[3]Borodulin, V. I., Gaponenko, V. R., Kachanov, Y. S., Meyer, D. G. W., Rist, U., Lian, Q. X., and Lee, C. B., "Late-Stage Transitional Boundary-Layer Structures. Direct Numerical Simulation and Experiment," *Theoretical and Computational Fluid Dynamics*, Vol. 15, No. 5, 2002, pp. 317–337.

[4]Herr, S., Wörner, A., Würz, W., Rist, U., and Wagner, S., "Experimental/Numerical Investigation of the Influence of a Pressure Gradient on Accoustic Roughness Receptivity in the Boundary Layer of an Airfoil," DGLR-Fachsymposium AG STAB, Stuttgart, Germany, Nov. 2000.

[5]Wagner, S., Kloker, M., and Rist, U. (eds.), "Recent Results in Laminar-Turbulent Transition," *Notes on Numerical Fluid Mechanics and Multidisciplinary Design*, Vol. 86, Springer-Verlag, Berlin, 2004, Chap. 4, pp. 231–292.

[6]Hausmann, F., "Heißfilmtechnik zur Transitionserkennung im Reiseflug," Ph.D. Dissertation, Dept. of Engineering, Aerodynamisches Inst., RWTH Aachen, Shaker, Germany, Feb. 2004.

[7]Hausmann, F., and Schröder, W., "Transition Detection in Cruise Flight Using a Resistant Multi-Sensor Hot-Film Technique," AIAA Paper 2004-1047, Jan. 2004.

[8]Hausmann, F., Schröder, W., and Limberg, W., "Development of a Multi-Sensor Hot-Film Measuring Technique for Transition Detection in Cruise Flight," AIAA Paper 2002-0534, Jan. 2002.

[9]Hausmann, F., Schröder, W., and Limberg, W., "A Hot-Film Measuring System for Free Flight Conditions," *Notes on Numerical Fluid Dynamics*, Vol. 86, Springer-Verlag, Berlin, 2004, pp. 281–292.

[10]Fühling, St., "Untersuchung Transitioneller, Ablösender und Gestörter Grenzschichten mit der Multisensor-Heißfilmtechnik," Ph.D. Dissertation, Aerodynamisches Inst., RWTH Aachen, Mainz, Germany, May 2000.

[11]Kornberger, M., "Multisensor-Heißfilmtechnik zur Transitionserkennung im Windkanal- und Flugversuch," Ph.D. Dissertation, Dept. of Engineering, Aerodynamisches Inst., RWTH Aachen, Shaker, Germany, Nov. 1992.

[12]Horstmann, K. H., Redeker, G., and Quast, A., "Flight Tests with a Natural Laminar Flow Glove on a Transport Aircraft," AIAA Paper 90-3044, Aug. 1990.

[13]Saric, W. S., and Reed, H. L., "Crossflow Instabilities—Theory & Technology," AIAA Paper 2003-0771, Jan. 2003.

[14]Pfenninger, W., "Flow Phenomena at the Leading-Edge of Swept Wings," AGARDograph, Vol. 97, May 1965.

[15]Pfenninger, W., "Laminar Flow Control—Laminarization," von Kármán Inst., AGARD, Rept. No. 654, Special Course on Drag Reduction, Rhode-St.-Genese, Belgium, June 1977.

[16]Dagenhart, J. R., and Saric, W. S., "Crossflow Stability and Transition Experiments in Swept-Wing Flow," NASA/TP-1999-209344, July 1999.